

Article

# Effects of Halogen, Chalcogen, Pnicogen, and Tetrel Bonds on IR and NMR Spectra

Jia Lu  and Steve Scheiner \* 

Department of Chemistry and Biochemistry, Utah State University, Logan, UT 84322-0300, USA

\* Correspondence: steve.scheiner@usu.edu

Received: 18 July 2019; Accepted: 31 July 2019; Published: 2 August 2019



**Abstract:** Complexes were formed pairing FX, FHY, FH<sub>2</sub>Z, and FH<sub>3</sub>T (X = Cl, Br, I; Y = S, Se, Te; Z = P, As, Sb; T = Si, Ge, Sn) with NH<sub>3</sub> in order to form an A···N noncovalent bond, where A refers to the central atom. Geometries, energetics, atomic charges, and spectroscopic characteristics of these complexes were evaluated via DFT calculations. In all cases, the A–F bond, which is located opposite the base and is responsible for the  $\sigma$ -hole on the A atom, elongates and its stretching frequency undergoes a shift to the red. This shift varies from 42 to 175 cm<sup>-1</sup> and is largest for the halogen bonds, followed by chalcogen, tetrel, and then pnicogen. The shift also decreases as the central A atom is enlarged. The NMR chemical shielding of the A atom is increased while that of the F and electron donor N atom are lowered. Unlike the IR frequency shifts, it is the third-row A atoms that undergo the largest change in NMR shielding. The change in shielding of A is highly variable, ranging from negligible for FSnH<sub>3</sub> all the way up to 1675 ppm for FBr, while those of the F atom lie in the 55–422 ppm range. Although smaller in magnitude, the changes in the N shielding are still easily detectable, between 7 and 27 ppm.

**Keywords:** stretching frequency; chemical shielding; atomic charge; NBO

## 1. Introduction

Recent years have witnessed a growing recognition of a range of newly rediscovered noncovalent bonds. Similarly to their closely related H-bond cousin, this class of bonds [1–25] are derived from a primary electrostatic attraction, supplemented by substantial amounts of charge transfer, polarization, and dispersion ingredients. In addition to their occurrence in small-model dimers, these sorts of interactions are a major factor in the structure and function of much larger supramolecular systems [26–35].

Rather than utilizing a H atom as a bridge between a pair of molecules, these related interactions incorporate a more electronegative atom, drawn from the right side of the periodic table. The primary difference from the H-bond is that this bridging atom does not have a partial positive charge which can draw in the negative region of an approaching nucleophile. Although the bridging atom may have an overall negative charge, its electrostatic potential is more complex, and quite anisotropic. Taking the R–X bond of halogen atom X as an example, the potential around X is characterized by a negative equator around the R–X bond, accompanied by a positive polar region lying along the extension of the R–X bond. This positive region, commonly referred to as a  $\sigma$ -hole, attracts the nucleophile in the same manner as the H atom within a H-bond.

Depending upon the family of elements from which this bridging atom is drawn, the resulting noncovalent bond is typically dubbed a halogen, chalcogen, pnicogen, or tetrel bond. These interactions share a number of features. Firstly, they are typically of a strength comparable to a H-bond, and are sometimes stronger by a substantial amount. Each such bond is systematically strengthened by electron-withdrawing substituents which intensify the  $\sigma$ -hole. These bonds are usually strengthened as one moves down each column of the periodic table, e.g., Cl < Br < I. First-row atoms, i.e., F, O, N,

and C, engage in only weak bonds of this type if at all, but can be coaxed into measurable interactions by appropriate substituents or adding a charge [36–42].

In the case of the H-bond, its spectroscopic consequences have been examined over a span of decades, and are well understood [43–46]. Such spectra are one of the tools used most often in the toolbox of chemists and biochemists in deciphering the interactions that are present in a complex system. Indeed, the shifts in certain IR spectroscopic bands or NMR peaks are frequently interpreted as a quantitative measure of the strength of each such bond. Work has also unraveled the source of these shifts, in terms of the most fundamental physical characteristics of the molecules involved. The surprise finding that certain H-bonds can shift an IR stretching frequency to the blue, rather than to the red which is the normal situation, has been analyzed and provided new insights into the source of this discrepancy [47–52].

However, while a good deal of information has accumulated in recent years concerning certain aspects of the halogen and related bonds, there is less information available concerning their spectra. The data that has appeared [36,53–62] has been informative, but does not consider these systems in a systematic manner. As such, currently, there is no thorough account of the manner in which each sort of interaction modulates the spectra, nor a solid understanding of the contributing factors. Such information would be crucial in detecting their presence in a given chemical or biological system. It would also be especially useful if correlations could be established, as is already the case with H-bonds, between certain spectroscopic parameters and the strength or geometry of a given bond.

The present work represents an attempt to fill this gap. A number of small-model systems are generated in which a halogen, chalcogen, pnictogen, or tetrel bond is present. Quantum calculations evaluate the strength of each interaction, as well as its geometric properties. The effects of each bond upon the IR and NMR spectra of the system are determined and compared with the binding strength, identity of the bond, and nature of the specific bridging atom. In this way, a systematic set of rules is generated that will assist in identification of these sorts of bonds in a complicated system, and to provide some measure of its strength.

## 2. Methods and Systems

In order to examine this question systematically, three different Lewis acids were considered for each type of bond. The central atom is drawn from the second, third, and fourth row of the periodic table, where these bonds are the strongest. An F atom was placed as a substituent on each such atom, as its electron-withdrawing power will facilitate the development of the noncovalent bond of interest. Thus, FCl, FBr, and FI were taken as prototype halogen bonding molecules. In a related manner, chalcogen bonds were considered via FSH, FSeH, and FTeH. The corresponding pnictogen and tetrel-bonding units are, respectively, (FPH<sub>2</sub>, FAsH<sub>2</sub>, FSbH<sub>2</sub>) and (FSiH<sub>3</sub>, FGeH<sub>3</sub>, FSnH<sub>3</sub>). NH<sub>3</sub> was taken as the common electron donor/nucleophile due, first, to its strength as a base. As a second benefit, its small size facilitates analysis and avoids complicating secondary interactions.

Calculations were carried out with the M06-2X variant [63] of DFT within the framework of the Gaussian 09 [64] suite of programs. The aug-cc-pVDZ basis set [65,66] was used for all atoms except fourth row I, Te, Sb and Sn, for which relativistic effects were incorporated via the aug-cc-pVDZ-PP pseudopotential [67,68]. The reliability of such methods applied in similar systems is supported by numerous previous works [69–75]. Geometries were optimized and harmonic frequency analysis assured the presence of a minimum.

Interaction energies,  $E_{\text{int}}$ , were taken as a measure of the strength of each interaction. This quantity refers to the difference in energy between the fully optimized complex and the energy sum of the two monomers, both in the geometry that pertains to the complex. This quantity was corrected for basis set superposition [76] by the counterpoise prescription [77], originally proposed by Boys and Bernardi. NMR chemical shielding was assessed via the GIAO procedure [78,79] incorporated within Gaussian. The Natural Bond Orbital (NBO) method [80] was utilized to extract natural atomic charges using the NBO-3.1 program, included within the Gaussian-09 program.

### 3. Results

The optimized geometries of several sample complexes are pictured in Figure 1. The others are quite similar and are contained in Figure S1. The  $\text{NH}_3$  approaches the central A atom of each molecule opposite to the A–F bond (where A denotes the halogen, chalcogen, etc., atom) although in the case of the chalcogen and pnictogen bonds, the  $\theta(\text{FA}\cdots\text{N})$  angle is not quite  $180^\circ$  due to considerations of the orientation of the  $\sigma$ -hole and secondary interactions [81–84]. It is the A–F bond of the Lewis acid molecule which ought to be most susceptible to modifications due to the interaction with the base, and where focus is placed below.

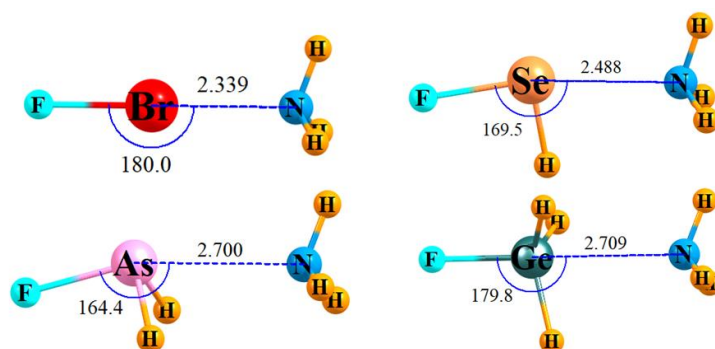


**Figure 1.** Geometries of sample noncovalently bonded complexes. Distance in Å and angles in degrees. The geometry that includes FSeH is not a pure minimum as it includes one negative frequency, which corresponds to torsional rotation of the  $\text{NH}_3$  group.

#### 3.1. Energetics and IR Spectra

The first column of Table 1 displays the interaction energy of each complex. It may be noted that these noncovalent bonds are all rather strong. To place this result in context, the water dimer, as a H-bonding parallel, has an interaction energy on the order of 5 kcal/mol [85,86]. The quantities in Table 1 are all larger than this amount, and in some cases are as much as four times larger.

**Table 1.** Interaction energy, NBO charge transfer energy, bond length change, and bond stretch frequency and intensity change upon forming complex with  $\text{NH}_3$ .

	$-E_{\text{int}}$ , kcal/mol	$E(2)$ , kcal/mol	$\Delta r$ (AF), Å	$\Delta \nu$ (AF), $\text{cm}^{-1}$	I Ratio <sup>a</sup>
halogen					
FCl	12.01	39.3	0.060	−174.9	7.7
FBr	16.28	51.3	0.061	−107.1	5.0
FI	19.17	43.6	0.055	−48.6	2.9
chalcogen					
FSH	9.12	21.0	0.034	−85.8	3.0
FSeH	12.25	30.9	0.042	−70.3	2.6
FTeH	16.14	20.9 <sup>b</sup>	0.042	−44.8	1.9
pnictogen					
FPH <sub>2</sub>	7.39	13.9	0.022	−58.1	1.9
FAsH <sub>2</sub>	8.98	16.3	0.029	−47.3	1.8
FSbH <sub>2</sub>	11.75	17.2	0.034	−42.1	1.5
tetrel					
FSiH <sub>3</sub>	9.01	18.1	0.027	−74.7	3.4
FGeH <sub>3</sub>	8.50	12.7	0.025	−55.2	1.6
FSnH <sub>3</sub>	12.18	13.3	0.030	−54.9	1.2

<sup>a</sup>  $I_{\text{complex}}/I_{\text{monomer}}$  for AF stretch, <sup>b</sup>  $\sigma(\text{Te-N}) \rightarrow \sigma^*(\text{Te-F})$ —NBO treats a complex as a single unit.

As is typically the case, each sort of interaction strengthens as the bridging atom, whether halogen, chalcogen, or otherwise, grows larger (with one minor exception for Ge vs. Si). In terms of the class of the bond, the halogen bonds are the strongest, followed by chalcogen, tetrel, and pnictogen. A common measure of the charge transfer taking place in each noncovalent bond derives from the NBO second-order perturbation energy  $E(2)$ . In each case, the donor is the N lone pair and the acceptor is the  $\sigma^*(A-F)$  antibonding orbital. These quantities in the second column of Table 1 generally follow the interaction energy trends, albeit imperfectly. For example, it is the second-row tetrel atom Si which shows a larger value of  $E(2)$  than either third- or fourth-row analogs. Third-row Br is associated with the largest  $E(2)$  of the three halogen atoms.

The transfer of electron density into the antibonding  $\sigma^*(A-F)$  bond ought to weaken and lengthen this bond, which can be seen by the stretches,  $\Delta r$ , documented in the third column of Table 1. As in the prior parameters,  $\Delta r$  follows the general pattern halogen > chalcogen > tetrel ~ pnictogen. This A–F bond weakening is also manifested in a red shift of the stretching frequency  $\Delta\nu$ . Like the energetics, the halogen > chalcogen > tetrel > pnictogen order also holds here. However, there is also a very significant difference. Unlike the energetics, these red shifts are largest for the lightest of each class of A atom. Taking the halogens as an example, this shift of  $175\text{ cm}^{-1}$  for Cl drops down to 107 for Br and then to 49 for I. However, perhaps most importantly, these shifts are all large enough that they ought to be plainly evident in the IR spectra of these systems, falling in the range of  $42\text{--}175\text{ cm}^{-1}$ .

As is typical of H-bonds, the red shift is accompanied by an intensification of the stretching band. The magnification of this intensity is displayed in the last column of Table 1 as the ratio of intensities in the complex and the monomer. This intensification ratio varies from as small as 1.2, up to 7.7 for  $\text{FCl}\cdots\text{NH}_3$ . This quantity decreases smoothly as each A atom becomes larger, and also follows the general pattern halogen > chalcogen > tetrel > pnictogen, which is very much in line with the red shifts,  $\Delta\nu$ .

### 3.2. NMR Shielding

The NMR chemical shielding of each of the salient atoms is reported in Table 2 as a change from the shielding within the uncomplexed monomer. While the shielding change in the central A atom is positive, its magnitude is highly variable. The halogen systems are a case in point. The shielding change on the I atom is 72 ppm, which rises to 478 ppm for Cl and then is dramatically larger at 1675 ppm for Br. Indeed, there does appear to be a pattern, in which the third-row atom in each class undergoes the largest change and the fourth-row atom, the smallest. The order observed here is fairly consistent with those in Table 1, with halogen the largest, followed by chalcogen. However, the pnictogen bonds clearly display larger NMR shifts than the tetrel atoms.

Unlike the increased shielding of the A atoms, the F substituents undergo a dramatic decrease, in the range between 55 and 422 ppm. However, the order is the same: halogen > chalcogen > pnictogen > tetrel. On the other hand, the dependence upon the particular row of the periodic table is erratic.  $\Delta\sigma$  clearly increases in magnitude as the halogen atom grows in size, but is less sensitive for the three other types of bonds.

Since the H atoms on the Lewis acid are not directly involved in the noncovalent bond, one would not anticipate their shielding to change much upon complexation. Nevertheless, while certainly smaller, these changes ought to be detectable. The H shielding increases in all cases: it is largest for the chalcogen bonds in the 4–5 ppm range, drops to about 1 ppm for pnictogen, and then below 0.5 ppm for the tetrel bonds.

As the electron donor atom, it is not surprising that the chemical shielding of the N atom of  $\text{NH}_3$  suffers a drop upon complexation. This decrease falls in the 7–27 ppm range so again, ought to be easily detectable. Unlike the other parameters discussed above, it is the tetrel bond that displays the largest perturbation for the N shielding change. The halogen bonds are somewhat less sensitive, followed by the two others. There is no clear pattern in terms of periodic table row. For example, while it is the lightest halogen atom that changes the N shielding the most, it is the heaviest of the pnictogen atoms that has this distinction.

**Table 2.** Changes in chemical shielding (ppm) that accompany complexation with NH<sub>3</sub>.

	A	F	H <sup>a</sup>	N
halogen				
FCl	478.2	−272.7	-	−20.2
FBr	1674.9	−391.2	-	−17.6
FI	72.3	−421.7	-	−6.9
chalcogen				
FSH	264.0	−184.1	3.8	−11.5
FSeH <sup>a</sup>	847.5	−234.0	4.9	−12.5
FTeH	34.8	−233.4	5.0	−8.3
pnicoen				
FPH <sub>2</sub>	68.2	−92.0	1.2	−10.6
FAsH <sub>2</sub>	165.9	−88.6	1.1	−8.7
FSbH <sub>2</sub>	5.0	−88.3	1.0	−12.4
tetrel				
FSiH <sub>3</sub>	46.3	−70.0	0.4	−26.6
FGeH <sub>3</sub>	70.7	−54.8	0.3	−16.3
FSnH <sub>3</sub>	−0.3	−59.7	0.3	−21.3

<sup>a</sup> average of all H atoms on the central atom.

### 3.3. Atomic Charges

One would expect that the shielding of each atom ought to have some relation with the total charge surrounding that atom. The changes in the atomic charge of each atom that accompany the complexation are thus displayed in Table 3. The negative values for the A atoms indicate an increased surrounding electron density, which is consistent with the greater shielding indicated in Table 2. On the other hand, the magnitudes of the charge changes bear little resemblance to the shielding. For example, the P, As, and Sb atoms all increase their negative charge by the same 0.035 e, yet there is a great variability in the shielding change, from 5 ppm for Sb to as high as 166 ppm for As. As an even greater disparity, the F atoms also accrue additional density during the complexation, comparable to that observed in A, but suffer a very substantial drop in their shielding, opposite to the increase in shielding in A.

The changes on the H atoms are small, 0.005 e or less, but vary in sign. While positive for the chalcogen and pnicoen bonds, they reverse sign for the tetrel bonds, even though the shielding change is positive for all systems. With respect to electron donor N, it suffers a loss of density, with its atomic charge growing more positive. However, this change is not universal, and is even negative for a few cases. There is some similarity to  $\Delta\sigma$  in that the most positive charge changes occur in the halogen bonds, which also display the largest change in N shielding. Both quantities are smaller for the chalcogen bonds. However, the small N-charge changes in the tetrel bonds are in dissonance with their large shielding changes.

### 3.4. Electron Density Shifts

A more thorough examination of the electron density shifts can perhaps offer some deeper insights into the changes in both atomic charges and NMR chemical shielding perturbations. Figure 2 displays the shifts in density caused by the complexation of NH<sub>3</sub> with FBr as an example. The purple regions represent gains of density and losses are shown in green. Two different levels are shown to provide a

more complete picture. The  $\Delta\rho = 0.001$  au contour is displayed in Figure 2a, while the larger value of 0.005 au in Figure 2b focuses attention on regions of more concentrated charge gain and depletion.

**Table 3.** Changes in natural atomic charge (e) that accompany complexation with  $\text{NH}_3$ .

	A	F	H <sup>a</sup>	N
halogen				
FCI	−0.076	−0.087	-	0.067
FBr	−0.084	−0.099	-	0.066
FI	−0.067	−0.086	-	0.031
chalcogen				
FSH	−0.044	−0.050	0.005	0.019
FSeH <sup>a</sup>	−0.058	−0.061	0.004	0.026
FTeH	−0.053	−0.056	0.001	0.007
pnictogen				
FPH <sub>2</sub>	−0.035	−0.029	0.003	0.003
FAsH <sub>2</sub>	−0.035	−0.034	0.002	0.001
FSbH <sub>2</sub>	−0.036	−0.035	−0.001	−0.007
tetrel				
FSiH <sub>3</sub>	−0.040	−0.028	−0.005	0.005
FGeH <sub>3</sub>	−0.016	−0.027	−0.005	−0.004
FSnH <sub>3</sub>	−0.012	−0.029	−0.010	−0.011

<sup>a</sup> average of all H atoms on central atom.

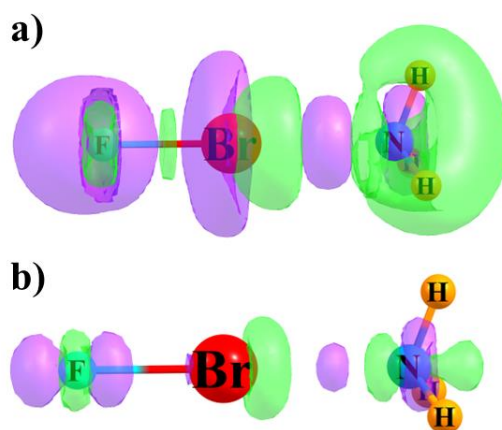


**Figure 2.** Density shifts caused by complexation between FBr and  $\text{NH}_3$ . Purple areas indicate gains and losses are shown in green. Contours shown represent (a) 0.001 au and (b) 0.005 au.

Considering the central Br atom first, in Figure 2a, a purple region of density gain to its left and a green area of density loss to its right are apparent. The former is larger than the latter which accounts for the more negative charge on the Br atom, as shown in Table 3. Consideration of only the 0.005 au contour in Figure 2b would offer a contrasting picture as the green area is much more extensive than the purple. The increased density around the Br atom is in part responsible for the higher NMR shielding indicated in Table 2. In the case of the N atom of  $\text{NH}_3$ , the green lobes of density loss appear to dominate at either contour value, which is consistent with the more positive charge of N in Table 3 and its reduced shielding in Table 2.

The F atom offers an interesting picture. One can see a green region of density loss close to the nucleus in Figure 2a, which is surrounded on both sides by two more extensive purple lobes of density gain. These areas persist in the more concentrated density loss regions shown in Figure 2b. As indicated in Table 3, it is the purple areas of gain that are more influential, as the overall charge on the F atom becomes more negative. On the other hand, the shielding of this atom is reduced substantially. One way of viewing this apparent paradox is consideration of the placement of these lobes. The green region of density loss occurs directly around the F nucleus, where this may have a more direct influence on the shielding than the more distant purple regions of density gain.

The density shifts of the  $\text{FBr} \cdots \text{NH}_3$  complex are not unique, but rather characteristic of all of the systems examined here. Comparable density shift diagrams are provided in Figure S2, where the similarities are evident.

#### 4. Discussion and Conclusions

Prior studies have provided confidence that NMR and IR data computed by DFT and ab initio approaches offer some reliability [38,58,87–90]. As a specific example, an early study [91] calculated nuclear shielding changes involved in the  $\text{P} \cdots \text{N}$  pnictogen bond in the  $\text{FH}_2\text{P} \cdots \text{NH}_3$  complex at the MP2/aug'-cc-pVTZ level. The P and N atoms changed their shielding by +77 and -10 ppm, respectively, which is similar to the quantities described here.

There have been several studies which have attempted to relate spectroscopic data with noncovalent bond energies. Mokrai et al. observed [92] through-space coupling constants within a pnictogen bond in solid-state NMR spectra. The NMR chemical shift of the C that is covalently attached to the halogen bonding I in a C–I bond increases markedly as the XB is enhanced by an anionic electron donor [93]. Within the framework of C–tetrel bonds, Southern and Bryce [38] observed a strong correlation between the C chemical shifts and the length of the C–tetrel bond, although this correlation deteriorated when compared to the actual strength of the bond. One should be cautious, however, in drawing parallels between observations in the broad context of noncovalent bonds in general and a limited set of tetrel bonds involving only the C atom, which tends to form weak tetrel bonds. As another point of agreement, the N electron donor of an aromatic ring suffers a decrease in its chemical shielding by a variable amount within a  $\text{CX} \cdots \text{N}$  halogen bond [94], up to as much as 19 ppm. As in the case of our  $\text{NH}_3$  electron donor, halogen bonding causes deshielding of the F atom when it acts as an electron donor in a halogen bond [95]. This is also consonant with our own findings, a red shift of the F–X stretching frequency has been observed [96] in its halogen bonds to aromatic N electron donors, in the range of about  $140 \text{ cm}^{-1}$ .

In summary, the noncovalent bonds that fall into the categories of halogen, chalcogen, pnictogen, and tetrel bonds have a number of spectroscopic features in common. As the base takes a position opposite the F–A bond of the  $\text{FH}_n\text{A}$  molecule, the covalent A–F bond is weakened and stretched by 0.025–0.060 Å. The stretching frequency of this bond is shifted to the red by at least  $40 \text{ cm}^{-1}$ , up to as much as  $175 \text{ cm}^{-1}$ . The amount of this red shift is largest for the A atoms of the second row of the periodic table: Cl, S, P, and Si. Halogen bonds cause the largest shift, followed by chalcogen, tetrel, and then pnictogen.

Each of the atoms involved in these bonds undergoes a characteristic change in its NMR signal. The shielding of the A atom is increased, while that of the F and electron donor N atom are lowered. The changes observed for the A and F atoms follow the order halogen > chalcogen > pnictogen > tetrel, but in the case of the N atom, the order changes to tetrel > halogen > chalcogen ~ pnictogen. Unlike the IR frequency shifts, it is the third-row A atoms that undergo the largest change in NMR shielding and the fourth row, the smallest. The latter small quantity contrasts with the fact that the interaction energies between the noncovalent bonds involving these heavy atoms are the largest. In terms of magnitude,  $\Delta\sigma$  for A is highly variable, ranging from negligible for  $\text{FSnH}_3$  all the way up to 1675 ppm for  $\text{FBr}$ . F shielding changes are not quite as variable, covering the range from 55 to 422 ppm. Although smaller in magnitude, the changes in the N shielding are still easily detectable, between 7 and 27 ppm.

**Supplementary Materials:** The following are available online at <http://www.mdpi.com/1420-3049/24/15/2822/s1>, Figure S1: Optimized geometry of complexes with NH<sub>3</sub>; Figure S2: Electron density shifts caused by complexation between Lewis acid and NH<sub>3</sub>.

**Author Contributions:** S.S. formulated the problem, and wrote a draft of the paper. J.L. performed the calculations and analysis.

**Funding:** This research received no external funding.

**Conflicts of Interest:** The authors declare no conflicts of interest.

## References

1. Del Bene, J.E.; Alkorta, I.; Elguero, J. Exploring N...C tetrel and O...S chalcogen bonds in HN(CH)SX:OCS systems, for X = F, NC, Cl, CN, CCH, and H. *Chem. Phys. Lett.* **2019**, *730*, 466–471. [[CrossRef](#)]
2. Gougoula, E.; Medcraft, C.; Alkorta, I.; Walker, N.R.; Legon, A.C. A chalcogen-bonded complex H<sub>3</sub>NS=C=S formed by ammonia and carbon disulfide characterised by chirped-pulse, broadband microwave spectroscopy. *J. Chem. Phys.* **2019**, *150*, 084307. [[CrossRef](#)] [[PubMed](#)]
3. Alkorta, I.; Legon, A. An Ab Initio Investigation of the Geometries and Binding Strengths of Tetrel-, Pnictogen-, and Chalcogen-Bonded Complexes of CO<sub>2</sub>, N<sub>2</sub>O, and CS<sub>2</sub> with Simple Lewis Bases: Some Generalizations. *Molecules* **2018**, *23*, 2250. [[CrossRef](#)] [[PubMed](#)]
4. Grabowski, S.J. Pnictogen and tetrel bonds—Tetrahedral Lewis acid centres. *Struct. Chem.* **2019**, *30*, 1141–1152. [[CrossRef](#)]
5. Grabowski, S. Tetrel Bonds with  $\pi$ -Electrons Acting as Lewis Bases—Theoretical Results and Experimental Evidences. *Molecules* **2018**, *23*, 1183. [[CrossRef](#)] [[PubMed](#)]
6. Alkorta, I.; Elguero, J.; Grabowski, S.J. Pnictogen and hydrogen bonds: Complexes between PH<sub>3</sub>X<sup>+</sup> and PH<sub>2</sub>X systems. *Phys. Chem. Chem. Phys.* **2015**, *17*, 3261–3272. [[CrossRef](#)]
7. Franconetti, A.; Quiñonero, D.; Frontera, A.; Resnati, G. Unexpected chalcogen bonds in tetravalent sulfur compounds. *Phys. Chem. Chem. Phys.* **2019**, *21*, 11313–11319. [[CrossRef](#)]
8. Franconetti, A.; Frontera, A. Theoretical and Crystallographic Study of Lead(IV) Tetrel Bonding Interactions. *Chem. Eur. J.* **2019**, *25*, 6007–6013. [[CrossRef](#)]
9. Frontera, A.; Bauzá, A. S...Sn Tetrel Bonds in the Activation of Peroxisome Proliferator-Activated Receptors (PPARs) by Organotin Molecules. *Chem. Eur. J.* **2018**, *24*, 16582–16587. [[CrossRef](#)]
10. Murray, J.S.; Politzer, P.  $\sigma$ -Holes and Si...N intramolecular interactions. *J. Mol. Model.* **2019**, *25*, 101. [[CrossRef](#)]
11. Clark, T.; Murray, J.S.; Politzer, P. A perspective on quantum mechanics and chemical concepts in describing noncovalent interactions. *Phys. Chem. Chem. Phys.* **2018**, *20*, 30076–30082. [[CrossRef](#)] [[PubMed](#)]
12. Riley, K.E.; Tran, K.-A. Strength, character, and directionality of halogen bonds involving cationic halogen bond donors. *Faraday Disc.* **2017**, *203*, 47–60. [[CrossRef](#)] [[PubMed](#)]
13. Riley, K.E.; Vazquez, M.; Umemura, C.; Miller, C.; Tran, K.-A. Exploring the (Very Flat) Potential Energy Landscape of R–Br... $\pi$  Interactions with Accurate CCSD(T) and SAPT Techniques. *Chem. Eur. J.* **2016**, *22*, 17690–17695. [[CrossRef](#)] [[PubMed](#)]
14. Scheiner, S. The pnictogen bond: Its relation to hydrogen, halogen, and other noncovalent bonds. *Acc. Chem. Res.* **2013**, *46*, 280–288. [[CrossRef](#)] [[PubMed](#)]
15. Zierkiewicz, W.; Michalczyk, M.; Wysokiński, R.; Scheiner, S. On the ability of pnictogen atoms to engage in both  $\sigma$  and  $\pi$ -hole complexes. Heterodimers of ZF<sub>2</sub>C<sub>6</sub>H<sub>5</sub> (Z = P, As, Sb, Bi) and NH<sub>3</sub>. *J. Mol. Model.* **2019**, *25*, 152. [[CrossRef](#)]
16. Zierkiewicz, W.; Michalczyk, M.; Wysokiński, R.; Scheiner, S. Dual Geometry Schemes in Tetrel Bonds: Complexes between TF<sub>4</sub> (T = Si, Ge, Sn) and Pyridine Derivatives. *Molecules* **2019**, *24*, 376. [[CrossRef](#)]
17. Zierkiewicz, W.; Fanfrlík, J.; Michalczyk, M.; Michalska, D.; Hobza, P. S...N chalcogen bonded complexes of carbon disulfide with diazines. Theoretical study. *Chem. Phys.* **2018**, *500*, 37–44. [[CrossRef](#)]
18. Dong, W.; Niu, B.; Liu, S.; Cheng, J.; Liu, S.; Li, Q. Comparison of  $\sigma$ -/ $\pi$ -Hole Tetrel Bonds between TH<sub>3</sub>F/F<sub>2</sub>TO and H<sub>2</sub>CX (X = O, S, Se). *ChemPhysChem* **2019**, *20*, 627–635.
19. Dong, W.; Wang, Y.; Cheng, J.; Yang, X.; Li, Q. Competition between  $\sigma$ -hole pnictogen bond and  $\pi$ -hole tetrel bond in complexes of CF<sub>2</sub>=CFZH<sub>2</sub> (Z = P, As, and Sb). *Mol. Phys.* **2019**, *117*, 251–259. [[CrossRef](#)]
20. Dong, W.; Li, Q.; Scheiner, S. Comparative Strengths of Tetrel, Pnictogen, Chalcogen, and Halogen Bonds and Contributing Factors. *Molecules* **2018**, *23*, 1681. [[CrossRef](#)]

21. Stasyuk, O.A.; Sedlak, R.; Guerra, C.F.; Hobza, P. Comparison of the DFT-SAPT and Canonical EDA Schemes for the Energy Decomposition of Various Types of Noncovalent Interactions. *J. Chem. Theory Comput.* **2018**, *14*, 3440–3450. [[CrossRef](#)] [[PubMed](#)]
22. Sedlak, R.; Eyrilmez, S.M.; Hobza, P.; Nachtigallova, D. The role of the s-holes in stability of non-bonded chalcogenide···benzene interactions: The ground and excited states. *Phys. Chem. Chem. Phys.* **2018**, *20*, 299–306. [[CrossRef](#)] [[PubMed](#)]
23. Esrafil, M.; Mousavian, P. Strong Tetrel Bonds: Theoretical Aspects and Experimental Evidence. *Molecules* **2018**, *23*, 2642. [[CrossRef](#)] [[PubMed](#)]
24. Scheiner, S.; Adhikari, U. Abilities of different electron donors (D) to engage in a P···D noncovalent interaction. *J. Phys. Chem. A* **2011**, *115*, 11101–11110. [[CrossRef](#)] [[PubMed](#)]
25. Esrafil, M.D.; Mousavian, P.; Mohammadian-Sabet, F. Tuning of pnictogen and chalcogen bonds by an aerogen-bonding interaction: A comparative ab initio study. *Mol. Phys.* **2019**, *117*, 58–66. [[CrossRef](#)]
26. Scilabra, P.; Terraneo, G.; Resnati, G. The Chalcogen Bond in Crystalline Solids: A World Parallel to Halogen Bond. *Acc. Chem. Res.* **2019**, *52*, 1313–1324. [[CrossRef](#)]
27. Kuwano, S.; Suzuki, T.; Yamanaka, M.; Tsutsumi, R.; Arai, T. Catalysis Based on C–I··· $\pi$  Halogen Bonds: Electrophilic Activation of 2-Alkenylindoles by Cationic Halogen-Bond Donors for [4 + 2] Cycloadditions. *Angew. Chem. Int. Ed.* **2019**, *58*, 10220–10224. [[CrossRef](#)]
28. Scheiner, S. Comparison of halide receptors based on H, halogen, chalcogen, pnictogen, and tetrel bonds. *Faraday Disc.* **2017**, *203*, 213–226. [[CrossRef](#)]
29. Dreger, A.; Wonner, P.; Engelage, E.; Walter, S.M.; Stoll, R.; Huber, S.M. A halogen-bonding-catalysed Nazarov cyclisation reaction. *Chem. Commun.* **2019**, *55*, 8262–8265. [[CrossRef](#)]
30. Trievel, R.C.; Scheiner, S. Crystallographic and Computational Characterization of Methyl Tetrel Bonding in S-Adenosylmethionine-Dependent Methyltransferases. *Molecules* **2018**, *23*, 2965. [[CrossRef](#)]
31. Vanderkooy, A.; Gupta, A.K.; Földes, T.; Lindblad, S.; Orthaber, A.; Pápai, I.; Erdélyi, M. Halogen Bonding Helicates Encompassing Iodonium Cations. *Angew. Chem. Int. Ed.* **2019**, *58*, 9012–9016. [[CrossRef](#)]
32. Pan, F.; Chen, Y.; Li, S.; Jiang, M.; Rissanen, K. Iodine Clathrated: A Solid-State Analogue of the Iodine–Starch Complex. *Chem. Eur. J.* **2019**, *25*, 7485–7488. [[CrossRef](#)]
33. Perera, M.D.; Aakeröy, C.B. Organocatalysis by a multidentate halogen-bond donor: An alternative to hydrogen-bond based catalysis. *New J. Chem.* **2019**, *43*, 8311–8314. [[CrossRef](#)]
34. Scheiner, S. Differential Binding of Tetrel-Bonding Bipodal Receptors to Monatomic and Polyatomic Anions. *Molecules* **2019**, *24*, 227. [[CrossRef](#)]
35. Scheiner, S. Assembly of Effective Halide Receptors from Components. Comparing Hydrogen, Halogen, and Tetrel Bonds. *J. Phys. Chem. A* **2017**, *121*, 3606–3615. [[CrossRef](#)]
36. Del Bene, J.E.; Alkorta, I.; Elguero, J. Anionic complexes of F<sup>−</sup> and Cl<sup>−</sup> with substituted methanes: Hydrogen, halogen, and tetrel bonds. *Chem. Phys. Lett.* **2016**, *655–656*, 115–119. [[CrossRef](#)]
37. Scheiner, S. Can two trivalent N atoms engage in a direct N···N noncovalent interaction? *Chem. Phys. Lett.* **2011**, *514*, 32–35. [[CrossRef](#)]
38. Southern, S.A.; Bryce, D.L. NMR Investigations of Noncovalent Carbon Tetrel Bonds. Computational Assessment and Initial Experimental Observation. *J. Phys. Chem. A* **2015**, *119*, 11891–11899. [[CrossRef](#)]
39. Scheiner, S. Comparison of CH···O, SH···O, Chalcogen, and Tetrel Bonds Formed by Neutral and Cationic Sulfur-Containing Compounds. *J. Phys. Chem. A* **2015**, *119*, 9189–9199. [[CrossRef](#)]
40. Vincent de Paul, N.N.; Scheiner, S. Comparison of p-hole tetrel bonding with s-hole halogen bonds in complexes of XCN (X = F, Cl, Br, I) and NH<sub>3</sub>. *Phys. Chem. Chem. Phys.* **2016**, *18*, 3581–3590. [[CrossRef](#)]
41. Liu, M.; Li, Q.; Scheiner, S. Comparison of tetrel bonds in neutral and protonated complexes of pyridineTF<sub>3</sub> and furanTF<sub>3</sub> (T = C, Si, and Ge) with NH<sub>3</sub>. *Phys. Chem. Chem. Phys.* **2017**, *19*, 5550–5559. [[CrossRef](#)]
42. Scheiner, S. Systematic Elucidation of Factors That Influence the Strength of Tetrel Bonds. *J. Phys. Chem. A* **2017**, *121*, 5561–5568. [[CrossRef](#)]
43. Hadzi, D.; Bratos, S. Vibrational Spectroscopy of the hydrogen bond. In *The Hydrogen Bond. Recent Developments in Theory and Experiments*; Schuster, P., Zundel, G., Sandorfy, C., Eds.; North-Holland Publishing Co.: Amsterdam, The Netherlands, 1976; Volume 2, pp. 565–611.
44. Gilli, G.; Gilli, P. *The Nature of the Hydrogen Bond*; Oxford University Press: Oxford, UK, 2009; p. 313.
45. Schuster, P.; Zundel, G.; Sandorfy, C. *The Hydrogen Bond. Recent Developments in Theory and Experiments*; North-Holland Publishing Co.: Amsterdam, The Netherlands, 1976.

46. Scheiner, S. *Hydrogen Bonding: A Theoretical Perspective*; Oxford University Press: New York, NY, USA, 1997; p. 375.
47. Hobza, P.; Havlas, Z. Blue-shifting hydrogen bonds. *Chem. Rev.* **2000**, *100*, 4253–4264. [[CrossRef](#)]
48. Masunov, A.; Dannenberg, J.J.; Contreras, R.H. C-H bond-shortening upon hydrogen bond formation: Influence of an electric field. *J. Phys. Chem. A* **2001**, *105*, 4737–4740. [[CrossRef](#)]
49. Gu, Y.; Kar, T.; Scheiner, S. Fundamental properties of the CH $\cdots$ O interaction: Is it a true hydrogen bond? *J. Am. Chem. Soc.* **1999**, *121*, 9411–9422. [[CrossRef](#)]
50. Qian, W.; Krimm, S. C-H $\cdots$ O and O-H $\cdots$ O hydrogen bonding in formic acid dimer structures: A QM/MM study confirms the common origin of their different spectroscopic behavior. *J. Phys. Chem. A* **2002**, *106*, 11663–11671. [[CrossRef](#)]
51. Jabłoński, M. Red and blue shifted hydridic bonds. *J. Comput. Chem.* **2014**, *35*, 1739–1747. [[CrossRef](#)]
52. Gu, Y.; Kar, T.; Scheiner, S. Comparison of the CH $\cdots$ N and CH $\cdots$ O interactions involving substituted alkanes. *J. Mol. Struct.* **2000**, *552*, 17–31. [[CrossRef](#)]
53. Bene, J.E.D.; Alkorta, I.; Elguero, J. Properties of cationic pnictogen-bonded complexes F $_4$ -nH $_n$ P $^+$ : N-base with H-P $\cdots$ N linear and n = 1–4. *Mol. Phys.* **2016**, *114*, 102–117. [[CrossRef](#)]
54. Ellington, T.L.; Reves, P.L.; Simms, B.L.; Wilson, J.L.; Watkins, D.L.; Tschumper, G.S.; Hammer, N.I. Quantifying the Effects of Halogen Bonding by Haloaromatic Donors on the Acceptor Pyrimidine. *ChemPhysChem* **2017**, *18*, 1267–1273. [[CrossRef](#)]
55. Esrafil, M.D.; Vakili, M. The effect of hydrogen-bonding cooperativity on the strength and properties of  $\sigma$ -hole interactions: An ab initio study. *Mol. Phys.* **2017**, *115*, 913–924. [[CrossRef](#)]
56. Gholipour, A.; Farhadi, S.; Neyband, R.S. Theoretical investigation of the nature and strength of simultaneous interactions of  $\pi$ - $\pi$  stacking and halogen bond including NMR, SAPT, AIM and NBO analysis. *Struct. Chem.* **2016**, *27*, 1543–1551. [[CrossRef](#)]
57. Cormanich, R.A.; Rittner, R.; O'Hagan, D.; Bühl, M. Inter- and intramolecular CF $\cdots$ C=O interactions on aliphatic and cyclohexane carbonyl derivatives. *J. Comput. Chem.* **2016**, *37*, 25–33. [[CrossRef](#)]
58. Viger-Gravel, J.; Leclerc, S.; Korobkov, I.; Bryce, D.L. Correlation between  $^{13}\text{C}$  chemical shifts and the halogen bonding environment in a series of solid para-diodotetrafluorobenzene complexes. *CrystEngComm* **2013**, *15*, 3168–3177. [[CrossRef](#)]
59. Alkorta, I.; Sánchez-Sanz, G.; Elguero, J.; Del Bene, J.E. Influence of hydrogen bonds on the P $\cdots$ P pnictogen bond. *J. Chem. Theory Comput.* **2012**, *8*, 2320–2327. [[CrossRef](#)]
60. Ma, N.; Zhang, Y.; Ji, B.; Tian, A.; Wang, W. Structural competition between halogen bonds and lone-pair $\cdots$ p interactions in solution. *ChemPhysChem* **2012**, *13*, 1411–1414. [[CrossRef](#)]
61. Jooneghani, S.G.N.; Gholipour, A. Mutual cooperation of  $\pi$ - $\pi$  stacking and pnictogen bond interactions of substituted monomeric Lawesson's reagent and pyridine rings: Theoretical insight into Pyr||X-PhPS2 $\perp$ pyr complexes. *Chem. Phys. Lett.* **2019**, *721*, 91–98. [[CrossRef](#)]
62. Watson, B.; Grounds, O.; Borley, W.; Rosokha, S.V. Resolving the halogen vs. hydrogen bonding dichotomy in solutions: Intermolecular complexes of trihalomethanes with halide and pseudohalide anions. *Phys. Chem. Chem. Phys.* **2018**, *20*, 21999–22007. [[CrossRef](#)]
63. Zhao, Y.; Truhlar, D.G. The M06 suite of density functionals for main group thermochemistry, thermochemical kinetics, noncovalent interactions, excited states, and transition elements: Two new functionals and systematic testing of four M06-class functionals and 12 other functionals. *Theor. Chem. Acc.* **2008**, *120*, 215–241.
64. Frisch, M.J.; Trucks, G.W.; Schlegel, H.B.; Scuseria, G.E.; Robb, M.A.; Cheeseman, J.R.; Scalmani, G.; Barone, V.; Mennucci, B.; Petersson, G.A.; et al. *Gaussian 09, Revision B.01*; Gaussian, Inc.: Wallingford, CT, USA, 2009.
65. Dunning, T.H.J. Gaussian basis sets for use in correlated molecular calculations. I. The atoms boron through neon and hydrogen. *J. Chem. Phys.* **1989**, *90*, 1007–1023. [[CrossRef](#)]
66. Woon, D.E.; Dunning, T.H., Jr. Gaussian basis sets for use in correlated molecular calculations. V. Core-valence basis sets for boron through neon. *J. Chem. Phys.* **1995**, *103*, 4572–4585. [[CrossRef](#)]
67. Feller, D. The role of databases in support of computational chemistry calculations. *J. Comput. Chem.* **1996**, *17*, 1571–1586. [[CrossRef](#)]
68. Schuchardt, K.L.; Didier, B.T.; Elsethagen, T.; Sun, L.; Gurumoorthi, V.; Chase, J.; Li, J.; Windus, T.L. Basis Set Exchange: A Community Database for Computational Sciences. *J. Chem. Infor. Model.* **2007**, *47*, 1045–1052. [[CrossRef](#)]

69. Ang, S.J.; Ser, C.T.; Wong, M.W. Modeling halogen bonding with planewave density functional theory: Accuracy and challenges. *J. Comput. Chem.* **2019**, *40*, 1829–1835. [[CrossRef](#)]
70. Orlova, A.P.; Jasien, P.G. Halogen bonding in self-assembling systems: A comparison of intra-and interchain binding energies. *Comput. Theor. Chem.* **2018**, *1139*, 63–69. [[CrossRef](#)]
71. Forni, A.; Pieraccini, S.; Franchini, D.; Sironi, M. Assessment of DFT Functionals for QTAIM Topological Analysis of Halogen Bonds with Benzene. *J. Phys. Chem. A* **2016**, *120*, 9071–9080. [[CrossRef](#)]
72. Bauzá, A.; García-Llinás, X.; Frontera, A. Charge-assisted triel bonding interactions in solid state chemistry: A combined computational and crystallographic study. *Chem. Phys. Lett.* **2016**, *666*, 73–78. [[CrossRef](#)]
73. Esrafil, M.D.; Vessally, E. A theoretical evidence for cooperative enhancement in aerogen-bonding interactions: Open-chain clusters of KrOF<sub>2</sub> and XeOF<sub>2</sub>. *Chem. Phys. Lett.* **2016**, *662*, 80–85. [[CrossRef](#)]
74. Mardirossian, N.; Head-Gordon, M. How Accurate Are the Minnesota Density Functionals for Noncovalent Interactions, Isomerization Energies, Thermochemistry, and Barrier Heights Involving Molecules Composed of Main-Group Elements? *J. Chem. Theory Comput.* **2016**, *12*, 4303–4325. [[CrossRef](#)]
75. Liao, M.S.; Lu, Y.; Scheiner, S. Performance assessment of density-functional methods for study of charge-transfer complexes. *J. Comput. Chem.* **2003**, *24*, 623–631. [[CrossRef](#)]
76. Latajka, Z.; Scheiner, S. Primary and secondary basis set superposition error at the SCF and MP2 levels: H<sub>3</sub>N–Li<sup>+</sup> and H<sub>2</sub>O–Li<sup>+</sup>. *J. Chem. Phys.* **1987**, *87*, 1194–1204. [[CrossRef](#)]
77. Boys, S.F.; Bernardi, F. The calculation of small molecular interactions by the differences of separate total energies. Some procedures with reduced errors. *Mol. Phys.* **1970**, *19*, 553–566. [[CrossRef](#)]
78. Ditchfield, R. GIAO studies of magnetic shielding in FHF<sup>−</sup> and HF. *Chem. Phys. Lett.* **1976**, *40*, 53–56. [[CrossRef](#)]
79. Alkorta, I.; Elguero, J. Ab initio hybrid DFT-GIAO calculations of the shielding produced by carbon-carbon bonds and aromatic rings in <sup>1</sup>H NMR spectroscopy. *New J. Chem.* **1998**, *22*, 381–385. [[CrossRef](#)]
80. Reed, A.E.; Curtiss, L.A.; Weinhold, F. Intermolecular interactions from a natural bond orbital, donor-acceptor viewpoint. *Chem. Rev.* **1988**, *88*, 899–926. [[CrossRef](#)]
81. Murray, J.S.; Resnati, G.; Politzer, P. Close contacts and noncovalent interactions in crystals. *Faraday Disc.* **2017**, *203*, 113–130. [[CrossRef](#)]
82. Adhikari, U.; Scheiner, S. The S···N noncovalent interaction: Comparison with hydrogen and halogen bonds. *Chem. Phys. Lett.* **2011**, *514*, 36–39. [[CrossRef](#)]
83. Adhikari, U.; Scheiner, S. Sensitivity of pnictogen, chalcogen, halogen and H-bonds to angular distortions. *Chem. Phys. Lett.* **2012**, *532*, 31–35. [[CrossRef](#)]
84. Scheiner, S. Detailed comparison of the pnictogen bond with chalcogen, halogen and hydrogen bonds. *Int. J. Quantum Chem.* **2013**, *113*, 1609–1620. [[CrossRef](#)]
85. Horn, P.R.; Mao, Y.; Head-Gordon, M. Probing non-covalent interactions with a second generation energy decomposition analysis using absolutely localized molecular orbitals. *Phys. Chem. Chem. Phys.* **2016**, *18*, 23067–23079. [[CrossRef](#)]
86. Schütz, M.; Brdarski, S.; Widmark, P.-O.; Lindh, R.; Karlström, G. The water dimer interaction energy: Convergence to the basis set limit at the correlated level. *J. Chem. Phys.* **1997**, *107*, 4597–4605. [[CrossRef](#)]
87. Alcívar León, C.D.; Echeverría, G.A.; Piro, O.E.; Ulic, S.E.; Jios, J.L.; Burgos Paci, M.; Argüello, G.A. The role of halogen C–X1···X2–C contact on the preferred conformation of 2-perhalomethylchromones in solid state. *Chem. Phys.* **2016**, *472*, 142–155. [[CrossRef](#)]
88. Chaudhary, P.; Goettel, J.T.; Mercier, H.P.A.; Sowlati-Hashjin, S.; Hazendonk, P.; Gerken, M. Lewis Acid Behavior of SF<sub>4</sub>: Synthesis, Characterization, and Computational Study of Adducts of SF<sub>4</sub> with Pyridine and Pyridine Derivatives. *Chem. Eur. J.* **2015**, *21*, 6247–6256. [[CrossRef](#)]
89. Hauchecorne, D.; van der Veken, B.J.; Herrebout, W.A.; Hansen, P.E. A <sup>19</sup>F NMR study of C–I···p halogen bonding. *Chem. Phys.* **2011**, *381*, 5–10. [[CrossRef](#)]
90. Pinheiro, P.D.S.M.; Rodrigues, D.A.; Alves, M.A.; Tinoco, L.W.; Ferreira, G.B.; de Sant’Anna, C.M.R.; Fraga, C.A.M. Theoretical and experimental characterization of 1,4-N···S s-hole intramolecular interactions in bioactive N-acylhydrazone derivatives. *New J. Chem.* **2018**, *42*, 497–505. [[CrossRef](#)]
91. Del Bene, J.E.; Alkorta, I.; Sanchez-Sanz, G.; Elguero, J. Structures, energies, bonding, and NMR properties of pnictogen complexes H<sub>2</sub>XP:NXH<sub>2</sub> (X = H, CH<sub>3</sub>, NH<sub>2</sub>, OH, F, Cl). *J. Phys. Chem. A* **2011**, *115*, 13724–13731. [[CrossRef](#)]

92. Mokrai, R.; Barrett, J.; Apperley, D.C.; Batsanov, A.S.; Benkő, Z.; Heift, D. Weak Pnictogen Bond with Bismuth: Experimental Evidence Based on Bi–P Through-Space Coupling. *Chem. Eur. J.* **2019**, *25*, 4017–4024. [[CrossRef](#)]
93. Szell, P.M.J.; Cavallo, G.; Terraneo, G.; Metrangolo, P.; Gabidullin, B.; Bryce, D.L. Comparing the Halogen Bond to the Hydrogen Bond by Solid-State NMR Spectroscopy: Anion Coordinated Dimers from 2- and 3-Iodoethynylpyridine Salts. *Chem. Eur. J.* **2018**, *24*, 11364–11376. [[CrossRef](#)]
94. Cerreia Vioglio, P.; Catalano, L.; Vasylyeva, V.; Nervi, C.; Chierotti, M.R.; Resnati, G.; Gobetto, R.; Metrangolo, P. Natural Abundance  $^{15}\text{N}$  and  $^{13}\text{C}$  Solid-State NMR Chemical Shifts: High Sensitivity Probes of the Halogen Bond Geometry. *Chem. Eur. J.* **2016**, *22*, 16819–16828. [[CrossRef](#)]
95. Thangavadivale, V.; Aguiar, P.M.; Jasim, N.A.; Pike, S.J.; Smith, D.A.; Whitwood, A.C.; Brammer, L.; Perutz, R.N. Self-complementary nickel halides enable multifaceted comparisons of intermolecular halogen bonds: Fluoride ligands vs. other halides. *Chem. Sci.* **2018**, *9*, 3767–3781. [[CrossRef](#)]
96. Masoodi, H.R.; Bagheri, S.; Ranjbar, M. Theoretical study of cooperativity between hydrogen bond–hydrogen bond, halogen bond–halogen bond and hydrogen bond–halogen bond in ternary FX ... diazine ... XF (X = H and Cl) complexes. *Mol. Phys.* **2016**, *114*, 3464–3474. [[CrossRef](#)]

**Sample Availability:** No compounds were synthesized.



© 2019 by the authors. Licensee MDPI, Basel, Switzerland. This article is an open access article distributed under the terms and conditions of the Creative Commons Attribution (CC BY) license (<http://creativecommons.org/licenses/by/4.0/>).